International Journal of Engineering

Journal Homepage: www.ije.ir

RESEARCH NOTE

Parametric Optimization of Electro Spark Microwelding of Aluminum Clad Steel

E. Rastkerdar[a], H. Aghajani*[a], A. Kianvash[a], C. C. Sorrell[b]

[a] *Department of Materials Engineering, University of Tabriz, Tabriz, East Azarbaijan, Iran*
[b] *School of Materials Science and Engineering, UNSW Australia, Sydney, NSW, Australia*

PAPER INFO

Paper history:
Received 28 Januray 2018
Received in revised form 19 February 2018
Accepted 09 March 2018

Keywords:
Electro Spark Microwelding
Aluminum Clad Steel
AA5183 Aluminum
Corrosion

ABSTRACT

The feasibility and parameters optimization of AA5183 aluminum cladding on AISI 1018 steel by electro spark microwelding (ESM) and the corrosion resistance of the clad plate were investigated. The optimum conditions were found as 15 A, 10%, 800 Hz and 2500 rpm for P, D, F and R factors, respectively. Confirmation test under optimum conditions showed that the model can be effectively used to predict the corrosion resistance of the aluminum clad steel. It appeared that higher cooling rates in the ESM process reduced the formation of detrimental precipitates owing to high intrinsic mutual affinity of Al and Fe. Excessive increase in the cooling rates was found to have a correlation to crack formation and reduced the corrosion resistance. Corrosion resistance of AA5183 aluminum clad AISI 1018 steel samples fabricated by ESM was a result of a compromise between the cooling rate and crack formation considerations in the clad.

***doi**: 10.5829/ije.2018.31.07a.20*

1. INTRODUCTION

Electro spark microwelding is a pulsed microwelding process [1] and also known as pulsed electrode surfacing (PES) [2], electro spark alloying (ESA) [3], electro spark coating (ESC) [4]. 5xxx wrought aluminum alloys offer good corrosion resistance (5% of the rate for bare low carbon steel in seawater), good weldability and high strength (~300 MPa depending on the composition and temper) [5]. The major alloying element in 5xxx aluminum alloys is magnesium which provides solid solution strengthening and additional strengthening through its influence on work hardening arising from cold deformation [6, 7].

AISI 1018 carbon steel contains about 0.18 wt.% carbon and 0.6–0.9 wt.% Mn. Although carbon steel has great qualities, it is well known that the corrosion resistance of carbon steels in the presence of moisture and chloride, and also the oxidation resistance at elevated temperatures, are relatively low [8]. Thus some cladding processes could be used to improve its corrosion resistance. ESM could be a promising technology to achieve the required corrosion properties in this steel. The present study was conducted to investigate the ESM of AA5183 aluminum clad AISI 1018 steel for corrosion resistance by optimizing four main control parameters of the process and by determining their consequent effects on the microstructure of the clad samples.

*Corresponding Author Email: *h_aghajani@tabrizu.ac.ir* (H. Aghajani)

2. MATERIALS AND METHODS

Rolled sheets of 2mm thick of AISI 1018 steel were cut into required sizes (10 mm×10 mm×2 mm). AA5183 rods by the chemical compositions of Al-5.20Mg-1.00Mn-0.25Si-0.40Fe-0.25Cr-0.25Zn-0.15Ti-0.05Cu-0.05Zr (wt.%) were used as clad metal i.e. ESM electrode. The nominal compositions of the AISI 1018 steel base metal was Fe-0.18C-0.90Mn-0.20Cr-0.40Si-0.04P-0.05S (wt.%). AA5183 aluminum rod and the steel sheets were in the annealed conditions. All samples were cladded with 400 µF capacitance. Argon with 99.999% purity was used as the shielding gas. Some of the experimental parameters were fixed from

Please cite this article as: E. Rastkerdar, H. Aghajani, A. Kianvash, C. Christopher Sorrell, Parametric Optimization of Electro Spark Microwelding of Aluminum Clad Steel, International Journal of Engineering (IJE), IJE TRANSACTIONS A: Basics Vol. 31, No. 7, (July 2018) 1146-1151

the trial runs so as to obtain sound clad samples. Cladding was performed using a device made by authors at University of Tabriz the features of which are shown in Figure 1. it is possible to calculate cooling rate of the workpiece through the cladding process of the base metal by Equation (1) [9].

$$\frac{dT}{dt} = 2\pi k \frac{(T_m - T_0)^2}{\frac{Q}{V}} \quad (1)$$

where, dT/dt (°C/s) is the cooling rate, T_m (°C) the melting point of the clad metal, T_0 (°C) the initial temperature of the base metal and Q/V (J/mm) is the heat input. The microstructures of the clad samples were examined with a scanning electron microscope (SEM, Hitachi S-3400X, Mito, Japan) equipped with energy dispersive X-ray spectrometer (EDS, Bruker QUANTAX, Billerica, MA). Electrochemical corrosion tests were carried out with a potentiostat (Parstat 2273) with a scan rate of 1 mV/s, a saturated calomel electrode (SCE) as a reference electrode and a platinum electrode as the counter electrode. The results of experiments were measured in terms of the width of the passive region (ΔE_{pit}) by Equation (2) as follows [10].

$$\Delta E_{pit} = E_{pit} - E_{corr} \quad (2)$$

3. RESULTS AND DISCUSSION

The 4 three-level factors are investigated in order to find the optimal levels to achieve the highest pitting corrosion resistance. The results of ΔE_{pit} measurements for all 27 samples in three replications are given in Table 1.

The experimental data was used to determine the average and signal to noise (S/N) analyses [11, 12]. Detailed information on all of the Taguchi calculation process achieved in this investigation could be found in the previous work of the authors [13].

From Table 1 and S/N ratio analysis, levels of the parameters (P,D,F,R)=(1,1,2,3) are as the best levels for reducing the variations of the ΔE_{pit} of AA5183 aluminum clad AISI 1018 steel. It must be noted that the distribution of factorial levels (1,1,2,3) was not one of the nine combinations tested in the present experiments. This is not unusual because of the small number of experiments conducted in the employed experimental design. In order to study the influence and significance of identified parameters, the analysis of variance (ANOVA) was performed on values of ΔE_{pit} and corresponding values of S/N ratio [14]. ANOVA analyses showed that the P, D, F and R affect the variability of ΔE_{pit} by 21.15, 34.83, 38.02, , and 6%, respectively. As shown in Figure 2, the thickness of the aluminum clad metal was approximately about 10 µm, and it appeared to be bonded metallurgically with AISI 1018 steel [15].

Figure 1. ESM device features manufactured by the authors at University of Tabriz

TABLE 1. Experimental results of ΔE_{pit} (mV) from three polarization test replications, average ΔE_{pit} (mV), corresponding MSD and S/N ratios for each distribution of four ESM parameters (P,D,F and R), (QC=bigger is better).

Trial No.	P (A)	D (%)	F (Hz)	R (rpm)	ΔE_{pit} (mV) Replication1	ΔE_{pit} (mV) Replication2	ΔE_{pit} (mV) Replication3	Average ΔE_{pit} (mV)	MSD	S/N ratio
1	15	10	500	1500	127	131	128	128.67	6.04E-05	42.19
2	15	30	800	2000	197	207	201	201.67	2.46E-05	46.09
3	15	50	1100	2500	135	141	140	138.67	5.21E-05	42.83
4	25	10	800	2500	177	183	185	181.67	3.03E-05	45.18
5	25	30	1100	1500	106	114	110	110.00	8.29E-05	40.82
6	25	50	500	2000	49	50	48	49.00	0.000417	33.80
7	35	10	1100	2000	162	172	166	166.67	3.61E-05	44.43
8	35	30	500	2500	118	120	117	118.33	7.14E-05	41.46
9	35	50	800	1500	110	117	113	113.33	7.8E-05	41.08
					Grand or Overall Average= 134.22					
					[S/N]M= 41.98					

The elemental scanning maps of the interfacial region in the aluminum clad are illustrated in Figure 2. Al, Fe, Mn and Si were found to be distributed in both the aluminum clad and steel.

According to Table 1, the lowest width of the passive region (ΔE_{pit} =48 mV) was observed at sample No. 6, the intermediate width of the passive region (ΔE_{pit} =128 mV) was observed at sample No. 1 and the highest width (ΔE_{pit} =201 mV) was observed at sample No. 2. Three potentiodynamic polarization curves of trial numbers 6, 1 and 2 (replication No. 3) are presented in Figure 3. The other polarization curves (24 curves) were similar to three polarization curves shown in Figure 3 but for brevity the other 24 polarization curves have not been presented here. Experimental results for the rate of heat generation (Q), energy of each spark (E_p), surface roughness (R_a), heat input (H.I.) and cooling rate (°C/s) for each distribution of four parameters (P,D,F and R) are given in Table 2.

From Figure 3, it can be observed that changing the ESM parameters only changed the corrosion potential (E_{corr}), without any significant changes in pitting nucleation potential (E_{pit}) . The E_{pit} is related to the characteristics of the Al-Mg matrix and is not dependent on the distribution of the precipitates. In other words, E_{pit} only reflects the crystallographic pitting behavior [16]. Figures 4(a), 4(b) and 4(c) show the SEM images of the aluminum clad metal at Trials No. 6, No.1 and No. 2 before exposure to 3.5% NaCl solution, respectively.

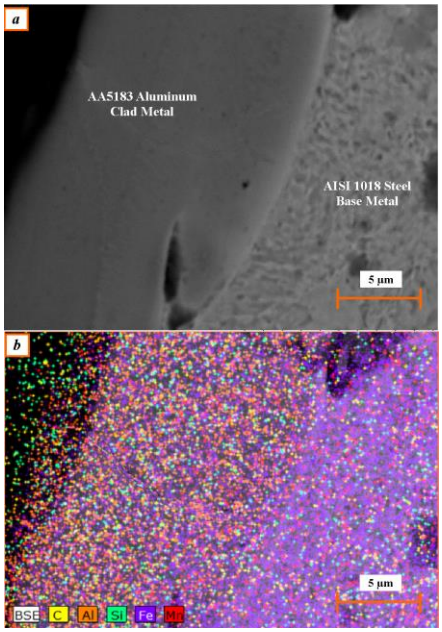

Figure 2. (a) SEM image showing the thickness (~10 µm) of the aluminum clad, (b) Elemental EDS maps for elements along the interface with the aluminum clad

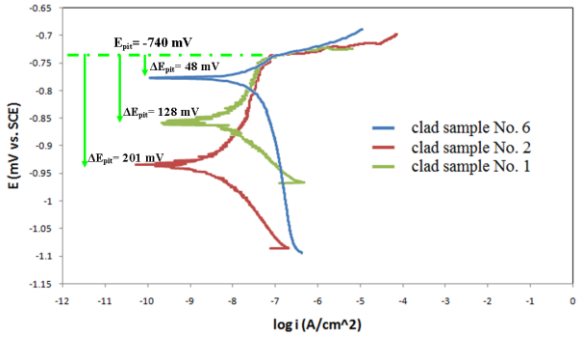

Figure 3. Potentiodynamic polarization curves in replication No. 3 corresponding to the three aluminum clad samples in different cladding conditions

TABLE 2. Experimental results for the rate of heat generation (Q), energy of each spark (E_p), roughness (Ra), heat input (H.I.) and cooling rate (°C/s) for each experimental set with variations in the four ESM parameters (P,D,F and R)

Trial No.	Q(W)	E_p (J)	Ra (µm)[a]	V(mm/s)	Heat Input (J/mm)	dT/dt ($\times 10^{-5}$ °C/s)
1	131	0.262	5.84	120	1.092	0.78
2	72	0.09	6.89	120	0.6	1.42
3	97.9	0.089	8.56	120	0.816	1.044
4	92.8	0.116	6.44	120	0.774	1.101
5	148.5	0.135	9.81	120	1.238	0.688
6	21	0.042	6.32	120	0.175	4.868
7	97.9	0.089	8.94	120	0.816	1.044
8	137.5	0.275	5.27	120	1.146	0.744
9	142.4	0.178	7.19	120	1.187	0.718

[a] Ra of the steel base metal before cladding, 0.35 µm

The SEM image in Figure 4 (d) shows the alkaline pits in sample No. 1 after the polarization test. The elemental scanning maps of Figure 4(a) also depicted in Figure 5. The different zones in these micrographs were analyzed by EDS in order to determine the type of intermetallics existing in these locations. The relative elemental ratios in the different zones clearly demonstrated that there were two different sorts of Al(Mn, Fe) and Al(Mg, Si) as compared to the aluminum matrix (Al-Mg). These intermetallic particles have been reported to play a major role on the pitting corrosion behavior of the AA5183 in 3.5 wt.% NaCl solution and are in accordance with pervious findings [17].

Volumetric fractions of the detrimental intermetallic precipitates presented in the clad metal of three samples were determined by image analysis of the SEM Image using Image Tool software [18].

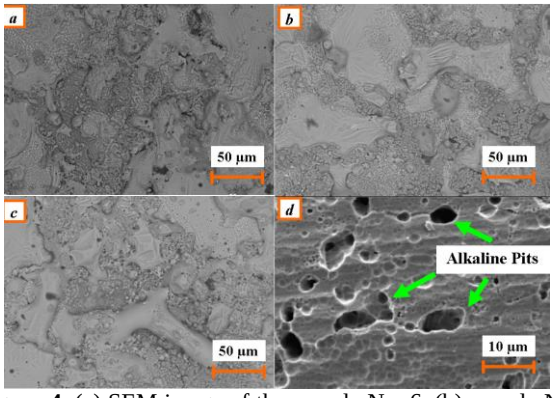

Figure 4. (a) SEM image of the sample No. 6, (b) sample No. 1, (c) sample No. 2 and (d) alkaline pits

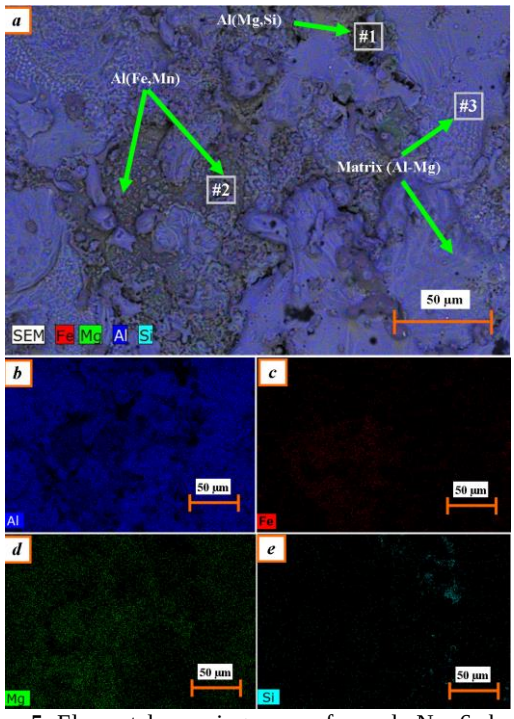

Figure 5. Elemental scanning maps of sample No. 6 showing (a) Al/Fe/Mg/Si elemental map, area #1 contains Al53.19-Mg27.66-Si19.15(wt.%), area #2 contains Al30.12-Fe64.16-Mn5.72, area #3 contains Al86.21-Mg6.03-O7.76 (b) Al elemental map, (c) Fe elemental map, (d) Mg elemental map and (e) Si elemental map

Among the three samples, the clad metal of sample No. 6 (Figure 4), with the cooling rate of 4.86 ($\times 10^5$ °C/s) (Table 2) was found to be decorated with the anodic and cathodic precipitates of Al(Mn, Fe) and Al(Mg, Si) about 25% and it showed the lowest width of the passive region in the polarization tests of 48 (mV vs. SCE). A decrease in cooling rate from 4.86 ($\times 10^5$ °C/s) in sample No. 6, to 0.78 ($\times 10^5$ °C/s) and 1.52 ($\times 10^5$ °C/s) (Table 2) in samples No. 1 and No. 2 caused an obvious increase in volumetric fractions of detrimental intermetallic precipitates to about 65 and 55% (Figures 4(b) and 4(c)), respectively. These results clearly showed that the volumetric fractions of detrimental precipitates decreased by increasing the cooling rate of the ESM process. Thus it would be expected that by increasing the cooling rates by means of changing the four parameters P, D, F and R, intermetallic formation decreases and pitting corrosion resistance increases.

However the sample No. 6 experienced the maximal cooling rate of 4.86 ($\times 10^5$ °C/s) and minimal volumetric fractions of ~25% among all samples but it showed the minimal pitting corrosion resistance of 48 (mV vs. SCE). Thus, it seemed that the advantage of the increasing of the cooling rate on increasing the pitting corrosion resistance via decreasing the volumetric fractions of anodic and cathodic precipitates was somewhat limited. Figure 6 shows the SEM micrograph of the cross sectional region of sample No. 6 with the highest cooling rate of 4.86 ($\times 10^5$ °C/s). It was obvious from Figure 6 that surface microcracks are present in the aluminum clad and it was clear that the minimal pitting corrosion resistance of 48 (mV vs. SCE) of this clad sample is related to these cracks. Thus by increasing the cooling rate there appeared to reach a maxima for corrosion resistance of the aluminum clad where the formation of the detrimental precipitates was hindered. By further increasing the cooling rates to excessive values, the microcrack formation in the aluminum clad tended to lower the corrosion resistance. It seems that too high cooling rates resulted in loss of metallurgical bonding between the different splats and promoted crack formation in the aluminum clad. Thus the pitting corrosion resistance of AA5183 aluminum clad AISI 1018 steel samples fabricated by ESM was dependent upon the cooling rates and formation of micro cracks in the clad. By changing the four parameters P, D, F and R, a verity of sound i.e. crack free or deficient AA5183 aluminum clad samples could be fabricated.

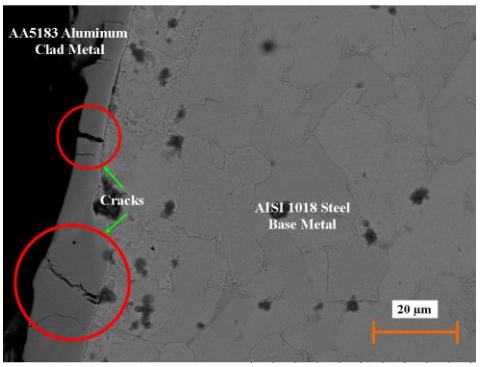

Figure 6. SEM micrograph of the cross section of sample No. 6 fabricated with the highest cooling rate of 4.86 ($\times 10^5$ °C/s)

In order to verify numerical conclusions, confirmation tests were performed and the results compared with the estimated performances. The confirmation test was performed by setting the optimal conditions of the four predominant factors P, D, F and R. Therefore, one AA5183 aluminum clad AISI 1018 steel was electro spark microwelded in (P,D,F,R)=(15 A, 10 %, 800 Hz, 2500 rpm) optimum condition. Polarization tests have been done three times on this sample. The value of ΔE_{pit} determined from three polarization curves were 225, 222 and 227 (mV vs. SCE). Figures 7(a) and 7(b) show the cross section of the clad interface and the microstructure of the clad with detrimental second phase particles of about 50 vol%, respectively. As can be seen in Figure 7(b) there are no visible cracks in the aluminum clad. Therefore, the confirmation test shows that there is a good agreement between predicted interval and experimental ΔE_{pit} values. It is an interesting idea to conduct more exact interfacial characterizations of AA5183 aluminum AISI 1018 steel interface of the electro spark microwelded clad in the optimized conditions calculated by Taguchi method throughout this paper for further researches.

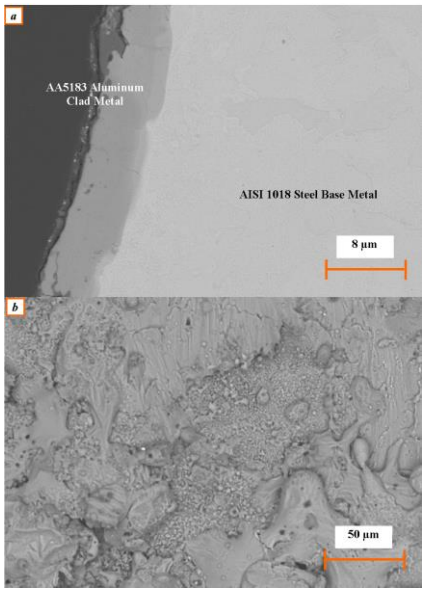

Figure 7. SEM micrograph of (a) the cross section and (b) the microstructure of the clad under optimized conditions.

4. CONCLUSIONS

Based on S/N ratio analysis, factors F and D with influence percent of 38.01 and 34.82%, respectively, had the most profound effect on the corrosion resistance. The confirmation test was carried out at optimal working conditions. ΔE_{pit} was increased to 225 (mV vs. SCE) by setting the control factors. The value of ΔE_{pit} in confirmation test fell in the predicted interval calculated from the Taguchi model and this shows that developed model can be effectively used to predict the ΔE_{pit} of ESM clad samples. Corrosion resistance of AA5183 aluminum clad AISI 1018 steel samples fabricated by ESM is a result of a compromise between cooling rate and cracks formation in the clad. High cooling rates in the ESM process reduces the formation of detrimental precipitates. However there appears to be a maxima value for such an increase in the cooling rate. Excessive increase in the cooling rates is seen to have a correlation to crack formation and this reduced the corrosion resistance.

5. REFERENCES

1. Radek, N. and Konstanty, N., "Cermet esd coatings modified by laser treatment", ***Archives of Metallurgy and Materials***, Vol. 57, No. 3, (2012), 665-670.
2. Staia, M., Fragiel, A., Cruz, M., Carrasquero, E., Campillo, B., Perez, R., Constantino, M. and Sudarshan, T., "Characterization and wear behavior of pulsed electrode surfacing coatings", ***Wear***, Vol. 251, No. 1, (2001), 1051-1060.
3. Chang-bin, T., Dao-xin, L., Zhan, W. and Yang, G., "Electro-spark alloying using graphite electrode on titanium alloy surface for biomedical applications", ***Applied Surface Science***, Vol. 257, No. 15, (2011), 6364-6371.
4. Raju, K.S., Faisal, N.H., Rao, D.S., Joshi, S. and Sundararajan, G., "Electro-spark coatings for enhanced performance of twist drills", ***Surface and Coatings Technology***, Vol. 202, No. 9, (2008), 1636-1644.
5. Jamal-Omidi, M. and Suki, M.M., "A numerical study on aluminum plate response under low velocity impact", ***International Journal of Engineering-Transactions C: Aspects***, Vol. 30, No. 3, (2017), 439-447.
6. Alijani, H. and Aboutalebi, F.H., "Evaluation of ductile damage criteria in hot forming processes", ***International Journal of Engineering-Transactions A: Basics***, Vol. 29, No. 10, (2016), 1441-1449.
7. Zarooni, M. and Eslami-farsani, R., "Effect of welding heat input on the intermetallic compound layer and mechanical properties in arc welding-brazing dissimilar joining of aluminum alloy to galvanized steel", ***International Journal of Engineering-Transactions B: Applications***, Vol. 29, No. 5, (2016), 669-676.
8. Depenyou, F., Doubla, A., Laminsi, S., Moussa, D., Brisset, J. and Le Breton, J.-M., "Corrosion resistance of aisi 1018 carbon steel in nacl solution by plasma-chemical formation of a barrier layer", ***Corrosion Science***, Vol. 50, No. 5, (2008), 1422-1432.
9. Kou, S., "Welding metallurgy", ***New York***, Vol., No., (1987).
10. Arenas, M., Bethencourt, M., Botana, F., De Damborenea, J. and Marcos, M., "Inhibition of 5083 aluminium alloy and galvanised steel by lanthanide salts", ***Corrosion Science***, Vol. 43, No. 1, (2001), 157-170.
11. Mehat, N.M. and Kamaruddin, S., "Optimization of mechanical properties of recycled plastic products via optimal processing parameters using the taguchi method", ***Journal of Materials Processing Technology***, Vol. 211, No. 12, (2011), 1989-1994.
12. Roy, R.K., "Design of experiments using the taguchi approach: 16 steps to product and process improvement, John Wiley & Sons, (2001).

13. Rastkerdar, E., Shamanian, M. and Saatchi, A., "Taguchi optimization of pulsed current gta welding parameters for improved corrosion resistance of 5083 aluminum welds", ***Journal of Materials Engineering and Performance***, Vol. 22, No. 4, (2013), 1149-1160.
14. Liu, W., Chien, W., Jiang, M. and Chen, W., "Study of nd: Yag laser annealing of electroless ni–p film on spiegel-iron plate by taguchi method and grey system theory", ***Journal of Alloys and Compounds***, Vol. 495, No. 1, (2010), 97-103.
15. Tang, S., Nguyen, T. and Zhou, Y., "Materials transfer in electro-spark deposition of tic p/ni metal-matrix composite coating on cu substrate", ***Welding Journal***, Vol. 89, No. 8, (2010), 172-180.
16. Aballe, A., Bethencourt, M., Botana, F., Marcos, M. and Sánchez-Amaya, J., "Influence of the degree of polishing of alloy aa 5083 on its behaviour against localised alkaline corrosion", ***Corrosion Science***, Vol. 46, No. 8, (2004), 1909-1920.
17. Aballe, A., Bethencourt, M., Botana, F. and Marcos, M., "Cecl 3 and lacl 3 binary solutions as environment-friendly corrosion inhibitors of aa5083 al–mg alloy in nacl solutions", ***Journal of Alloys and Compounds***, Vol. 323, (2001), 855-858.
18. "Image tool version 3.0, university of texas health science center at san antonio, free software, available in http:// ddsdx.Uthscsa.Edu/dig/itdesc.Html. Access in 09.03.2007",

Parametric Optimization of Electro Spark Microwelding of Aluminum Clad Steel

RESEARCH NOTE

E. Rastkerdar[a], H. Aghajani[a], A. Kianvash[a], C. C. Sorrell[b]

[a] *Department of Materials Engineering, University of Tabriz, Tabriz, East Azarbaijan, Iran*
[b] *School of Materials Science and Engineering, UNSW Australia, Sydney, NSW, Australia*

P A P E R I N F O

Paper history:
Received 28 Januray 2018
Received in revised form 19 February 2018
Accepted 09 March 2018

Keywords:
Electro Spark Microwelding
Aluminum Clad Steel
AA5183 Aluminum
Corrosion

چکیده

امکان‌سنجی و بهینه‌سازی پارامترهای روکش‌کاری آلومینیوم AA5183 بر روی فولاد AISI 1018 با فرایند میکروجوشکاری جرقه الکتریکی (ESM) و مقاومت به خوردگی صفحه روکش شده مورد بررسی قرار گرفت. شرایط بهینه برای چهار پارامتر P، D، F و R به ترتیب 15 A، 10٪، 800 Hz و 2500 rpm به دست آمد. آزمون تایید در شرایط بهینه نشان داد که مدل ارایه شده می‌تواند به طور موثر برای پیش‌بینی مقاومت به خوردگی فولاد روکش شده با آلومینیوم استفاده شود. مشاهده شد که نرخ‌های بالای سرد شدن بالاتر در فرایند ESM، تشکیل رسوب‌های مخرب ولی اجتناب‌ناپذیر حاصل از میل ترکیبی بالای Al و Fe به یکدیگر را کاهش می‌دهد. مشاهده شد که نرخ‌های سرد شدن بیش از حد بالا منجر به تشکیل ترک‌ها و کاهش مقاومت به خوردگی خواهند شد. مقاومت به خوردگی نمونه‌های آلومینیوم AA5183 بر روی فولاد AISI 1018 ساخته شده توسط فرایند ESM نتیجه یک مصالحه میان نرخ سرد شدن و تشکیل ترک در روکش ایجاد شده بودند.

***doi**: 10.5829/ije.2018.31.07a.20*